Spin polarization and color superconductivity in quark matter

E. Nakano
Department of Physics, Tokyo Metropolitan University, 1-1 Minami-Ohsawa, Hachioji, Tokyo 192-0397, Japan

T. Maruyama
College of Bioresource Sciences, Nihon University, Fujisawa 252-8510, Japan;
Japan Atomic Energy Research Institute, Tokai, Ibaraki 319-1195, Japan;
and Institute for Quantum Energy, Nihon University, Chiyoda-ku, Tokyo 101-8308, Japan

T. Tatsumi
Department of Physics, Kyoto University, Kyoto 606-8502, Japan
(Received 10 April 2003; published 3 November 2003)

A coexistent phase of spin polarization and color superconductivity in high-density QCD is investigated using a self-consistent mean-field method at zero temperature. The axial-vector self-energy stemming from the Fock exchange term of the one-gluon-exchange interaction has a central role in causing spin polarization. The magnitude of spin polarization is determined by the coupled Schwinger-Dyson equations with a superconducting gap function. As a significant feature, the Fermi surface is deformed by the axial-vector self-energy and then rotation symmetry is spontaneously broken down. The gap function results in being anisotropic in the momentum space in accordance with the deformation. As a result of numerical calculations, it is found that spin polarization barely conflicts with color superconductivity, but almost coexists with it.

DOI: 10.1103/PhysRevD.68.105001 PACS number(s): 12.38.Mh, 05.30.Fk, 67.60.−g

I. INTRODUCTION

Recently, there has been a lot of interest in high-density QCD, especially in quark Cooper-pair condensation phenomena at high-density quark matter [called color superconductivity (CSC)], in connection with, e.g., physics of heavy ion collisions and neutron stars [1–3]. Its mechanism is similar to the BCS theory for the electron-phonon system [4], in which the attractive interaction of electrons is provided by phonon exchange and causes Cooper instability near the Fermi surface. As for quark matter, the quark-quark interaction is mediated by colored gluons, and is often approximated by some effective interactions, e.g., the one-gluon-exchange (OGE) or the instanton-induced interaction, both of which give rise to the attractive quark-quark interaction in the color antisymmetric **3*** channel. CSC leads to spontaneous symmetry breaking of color $SU(3)$ into $SU(2)$ as a result of condensation of quark Cooper pairs [2,3].

In this paper we would like to address another phenomenon expected in quark matter: spin polarization or ferromagnetism of quark matter. We examine the possibility of the spin-polarized phase with CSC in quark matter. As far as we know, the interplay between the color superconducting phase and other phases characterized by the nonvanishing mean fields of the spinor bilinears $\langle\bar{\psi}\Gamma\psi\rangle$ has not been explored except for the case of chiral symmetry breaking [5]. Our main concern here is to investigate the possibility of quark Cooper instability under the axial-vector mean field, $\langle\bar{\psi}\gamma^{\mu}\gamma_5\psi\rangle$ which is responsible for spin polarization of quark matter. It would be worth mentioning in this context that ferromagnetism (or spin polarization) and superconductivity are fundamental concepts in condensed matter physics, and their coexistent phase has been discussed for a long time [6]. In recent progress, a superconducting phase has been discovered in ferromagnetic materials and much effort has been made to understand the coexisting mechanism [7].

In addition to being interesting in its own right, the coexistence problem may be related to some physical phenomena. Recently, a new type of neutron stars, called as ''magnetars,'' with a super strong magnetic field of $\sim O(10^{15}$ G) has been discovered [8,9]. They may raise an interesting question for the origin of the magnetic field in compact stars, since its strength is too large to regard it as a successor from progenitor stars, unlike canonical neutron stars [10]. Since hadronic matter spreads over inside neutron stars beyond the nuclear density ($\rho_0 \sim 0.16$ fm^{-3}), it should be interesting to consider the microscopic origin of the magnetic field in magnetars. In this context, a possibility of ferromagnetism in quark matter due to the OGE interaction has been suggested by one of the authors (T.T.) within a variational framework [11]; a competition between the kinetic and the Fock exchange energies gives rise to spin polarization, similarly to Bloch's idea for itinerant electrons. Salient features of spin polarization in the relativistic system are also discussed in Ref. [11]. Thus, it might be also interesting to examine the possibility of the spin-polarized phase with CSC in quark matter, in connection with magnetars.

We investigate spin polarization in the color superconducting phase by a self-consistent framework, in which quark Cooper pairs are formed under the axial-vector mean-field. We shall see that this phenomenon is a manifestation of spontaneous breaking of both color $SU(3)$ and rotation symmetries.

We adopt here the OGE interaction as an effective quark-quark interaction. Since the Fermi momentum is very large at high density, asymptotic freedom of QCD implies that the interaction between quarks is very weak [12]. So it may be

reasonable to think that the OGE interaction has a dominant contribution for the quark-quark interaction. In the framework of relativistic mean-field theories, the axial-vector and tensor mean fields, which stem from the Fock exchange terms, $\langle\bar{\psi}\gamma_5\gamma_\mu\psi\rangle$ and $\langle\bar{\psi}\sigma_{\mu\nu}\psi\rangle$, may have a central role to split the degenerate single-particle energies of the two spin states, and then leads to spin polarization, e.g., see [13] for discussion in nuclear matter. As for quark matter, several types of the color singlet mean-fields appear after the Fierz transformation in the Fock exchange terms, but we retain only the axial-vector mean-field as the origin of spin polarization, because the OGE interaction by no means holds the tensor mean field due to chiral symmetry in QCD, unlike nuclear matter [13]. Presence of the axial-vector mean-field deforms the quark Fermi seas according to their spin degrees of freedom, and thereby the gap function should be no more isotropic in the momentum space. We assume here an anisotropic gap function Δ on the Fermi surface by a physical consideration and solve the coupled Schwinger-Dyson equations self-consistently by way of the Nambu formalism to find the axial-vector mean-field U_A and the superconducting gap function Δ. Thus we discuss the interplay between spin polarization and superconductivity in quark matter.

In Sec. II we give a framework to deal with the present subject. The explicit structure of the anisotropic gap function Δ in the color, flavor, and Dirac spaces is carefully discussed there and in the Appendix B and Appendix C. Numerical results about U_A and Δ are given in Sec. III, where phase diagram of spin polarization and color superconductivity is given in the mass-baryon number density plane. Section IV is devoted to summary and concluding remarks.

II. FORMALISM

In this section we present our formalism to treat CSC and spin polarization. We consider quark matter with flavor $SU(2)$ and color $SU(3)$ symmetries, and assume that the interaction action is described by the OGE interaction as

$$I_{int}=-g^2\frac{1}{2}\int \mathrm{d}^4x\int \mathrm{d}^4y\left[\bar{\psi}(x)\gamma^\mu\frac{\lambda_a}{2}\psi(x)\right]\times D_{\mu\nu}(x,y)\left[\bar{\psi}(y)\gamma^\nu\frac{\lambda_a}{2}\psi(y)\right], \tag{1}$$

where ψ is the quark field, $D_{\mu\nu}(x,y)$ is the gauge boson (gluon) propagator, and $\lambda_a\,(a=1,2,\ldots,8)$ are the $SU(3)$ Gell-Mann matrices. Using the Nambu formalism [2,14] the effective action is given within the mean-field approximation as

$$I_{MF}=\frac{1}{2}\int\frac{\mathrm{d}^4p}{(2\pi)^4}\begin{pmatrix}\bar{\psi}(p)\\ \bar{\psi}_c(p)\end{pmatrix}^T G^{-1}(p)\begin{pmatrix}\psi(p)\\ \psi_c(p)\end{pmatrix} \tag{2}$$

with the inverse quark Green function

$$G^{-1}(p)=\begin{pmatrix}\not{p}-m+\not{\mu}+V(p) & \gamma_0\Delta^\dagger(p)\gamma_0\\ \Delta(p) & \not{p}-m-\not{\mu}+\bar{V}(p)\end{pmatrix}, \tag{3}$$

where $\not{\mu}=\gamma_0\mu$ with the chemical potential μ. V is a self-energy and Δ is the gap function for the quark Cooper pair; both terms V and Δ should be provided by the Fock exchange terms of the OGE interaction. We define here $\psi_c(k)$ and $\bar{V}$ as

$$\psi_c(k)=C\bar{\psi}^T(-k), \tag{4}$$

$$\bar{V}\equiv CV^TC^{-1} \tag{5}$$

with the charge conjugation matrix C which is explicitly given by $i\gamma_2\gamma_0$ in Dirac representation.

The Green function $G(p)$ can be written straightforwardly from Eq. (3) as

$$G(p)=\begin{pmatrix}G_{11}(p) & G_{12}(p)\\ G_{21}(p) & G_{22}(p)\end{pmatrix} \tag{6}$$

with

$$G_{11}(p)=\{\not{p}-m+\not{\mu}+V(p)-\gamma_0\Delta(p)^\dagger\gamma_0[\not{p}-m-\not{\mu}+\bar{V}(p)]^{-1}\Delta(p)\}^{-1}, \tag{7}$$

$$G_{21}(p)=-[\not{p}-m-\not{\mu}+\bar{V}(p)]^{-1}\Delta(p)G_{11}(p). \tag{8}$$

Following Nambu's argument [14], we impose the self-consistency condition to obtain the Hartree-Fock ground state such that the self-energy by the residual interaction, $\Sigma_{Res.}$, vanishes,

$$\Sigma_{Res}=\Sigma_{MF}-\Sigma_{Int}=0, \tag{9}$$

where Σ_{MF} is defined by

$$\Sigma_{MF}(k)=G_0^{-1}(k)-G^{-1}(k)=-\begin{pmatrix}V(k) & \gamma_0\Delta^\dagger(k)\gamma_0\\ \Delta(k) & \bar{V}(k)\end{pmatrix} \tag{10}$$

with

$$G_0(p)=\begin{bmatrix}(\not{p}-m+\not{\mu})^{-1} & 0\\ 0 & (\not{p}-m-\not{\mu})^{-1}\end{bmatrix}, \tag{11}$$

and Σ_{Int} is given by the use of the OGE interaction. Within the first-order approximation in g^2, Σ_{Int} renders

$$\Sigma_{Int}(k)=g^2\int\frac{\mathrm{d}^4p}{i(2\pi)^4}D^{ab}(k-p)\hat{\Gamma}_aG(p)\hat{\Gamma}_b \tag{12}$$

$$\hat{\Gamma}_a \equiv \begin{pmatrix} \gamma^\mu \frac{\lambda_\alpha}{2} & 0 \\ 0 & C\left(\gamma^\mu \frac{\lambda_\alpha}{2}\right)^T C^{-1} \end{pmatrix} = \begin{pmatrix} \gamma^\mu \frac{\lambda_\alpha}{2} & 0 \\ 0 & -\gamma^\mu \frac{\lambda_\alpha^T}{2} \end{pmatrix}, \tag{13}$$

which is nothing else but the Fock exchange energy by the OGE interaction. Using Eqs. (9)–(12), we obtain the self-consistent equation for $V(k)$ by the use of the diagonal component of the full Green function (7),

$$-V(k) = (-ig)^2 \int \frac{d^4p}{i(2\pi)^4} [-iD^{\mu\nu}(k-p)] \gamma_\mu \times \frac{\lambda_\alpha}{2} [-iG_{11}(p)] \gamma_\nu \frac{\lambda_\alpha}{2}. \tag{14}$$

The gap equation is also obtained from the off-diagonal component as

$$-\Delta(k) = (-ig)^2 \int \frac{d^4p}{i(2\pi)^4} [-iD^{\mu\nu}(k-p)] \times \gamma_\mu \frac{-(\lambda_\alpha)^T}{2} [-iG_{21}(p)] \gamma_\nu \frac{\lambda_\alpha}{2}. \tag{15}$$

In the following sections, we present explicit forms of $V(p)$ and $\Delta(p)$ and then solve their coupled equations (14) and (15).

A. Fermion propagator under the axial-vector self-energy

We, hereafter, take the static approximation for the gauge-boson propagator as

$$D_{\mu\nu}(q) \approx -\frac{g_{\mu\nu}}{\mathbf{q}^2 + M^2} \tag{16}$$

where M is an effective gauge boson mass originated from the Debye screening $M^2 \sim N_f g^2 \mu^2/(2\pi^2)$ [15].

Since typical momentum transfer $|\mathbf{q}|$ at high density is of the order of the chemical potential, we may further introduce the zero-range approximation [16] for the propagator as

$$D_{\mu\nu}(q) \approx -\frac{g_{\mu\nu}}{Q^2 + M^2}, \tag{17}$$

with a typical momentum scale Q of $O(\mu)$. This approximation corresponds to the Stoner model [17], which is popular in solid-state physics, and stands on the same concept of the NJL model [18] as well.

To proceed, we assume, without loss of generality, that total spin expectation value is oriented to the negative z direction in the spin-polarized phase which is caused by the finite axial-vector mean-field along the z axis.[1] As shown in Ref. [13], rotation symmetry is spontaneously broken down in this phase while axial symmetry around the z axis is preserved. Then two Fermi seas of the different spin states are deformed accordingly.

Applying the Fierz transformation for the Fock exchange energy term (14) we can see that there appear the color-singlet scalar, pseudoscalar, vector and axial-vector self-energies (Appendix D). In general we must take into account these self-energies in V, $V = U_s + i\gamma_5 U_{ps} + \gamma_\mu U_v^\mu + \gamma_\mu \gamma_5 U_{av}^\mu$ with the mean-fields U_α. Here we introduce an ansatz: the Femri distribution holds the reflection symmetry with respect to the $p_x - p_y$ plane, and only the mean-field parts U_s, U_v^0 and U_{av}^3 are retained in V. Later we will see that the self-consistent solution is obtained with the zero-range approximation (17) under this ansatz.

In this paper, furthermore, we disregard the scalar mean-field U_s and the time component of the vector mean-field U_v^0 for simplicity since they are irrelevant for the spin degree of freedom; U_v^0 has only a role to shift the total energy to the chemical potential, and may not affect any other physical properties. On the other hand, U_s may significantly influence the spin-polarization properties through changing the quark effective mass. Instead of introducing the scalar mean-field explicitly, however, we treat the quark mass as a variable parameter, and discuss its effect in the next section.

According to the above assumptions and considerations the self-energy V in Eq. (3) renders

$$V = \gamma_3 \gamma_5 U_A, \quad U_A \equiv U_{av}^3, \tag{18}$$

with the axial-vector mean-field U_A. Then the diagonal component of the Green function $G_{11}(p)$ is written as

$$G_{11}(p) = [G_A^{-1} - \gamma_0 \Delta^\dagger \gamma_0 \tilde{G}_A \Delta]^{-1} \tag{19}$$

with

$$G_A^{-1}(p) = \not{p} - m + \not{\mu} - \gamma_5 \gamma_3 U_A, \tag{20}$$

$$\tilde{G}_A^{-1}(p) = \not{p} - m - \not{\mu} - \overline{\gamma_5 \gamma_3} U_A, \tag{21}$$

where $\overline{\gamma_5 \gamma_3} = \gamma_5 \gamma_3$ and $G_A(p)$ is the Green function with the axial-vector mean-field U_A which is determined self-consistently by way of Eq. (14).

Before constructing the gap function Δ, we first find the single-particle spectra and their eigenspinors in the absence of Δ, which is achieved by diagonalization of the operator G_A^{-1}. In the usual case of no spin polarization this procedure gives nothing but the free energy spectra and plane waves. Then we choose a gap structure on the basis of a physical consideration as in the usual BCS theory.

[1] We shall see that only the space component of the axial-vector mean field is responsible for spin polarization. Hereafter, we take its direction along the z axis without loss of generality.

From the condition that $\det G_A^{-1}(p_0)|_{\mu=0}=0$ one can obtain four single-particle energies $\epsilon_\pm$ (positive energies) and $-\epsilon_\pm$ (negative energies), which are given as

$$\epsilon_\pm(\boldsymbol{p})=\sqrt{\boldsymbol{p}^2+U_A^2+m^2\pm 2U_A\sqrt{m^2+p_z^2}}, \tag{22}$$

where the sign factor ± 1 being in front of U_A indicates the energy splitting between different spin states due to the presence of the axial-vector self-energy, which corresponds to the *exchange splitting* in the non-relativistic electron system [17]. In the following, we call the "spin"-up (-down) states for the states $\pm\epsilon_+$ ($\pm\epsilon_-$). Equation (22) also shows that each Fermi sea for the "spin"-up (-down) state should undergo a deformation and lose rotation symmetry, once U_A is finite. This is a genuine relativistic effect [13]; actually the exchange splitting never produces deformation of the Fermi sea in the nonrelativistic ferromagnetism, e.g., in the Stoner model [17].

Here, it would be interesting to see the peculiarities of the quark Fermi seas in the presence of the axial-vector self-energy. In Fig. 1 we sketch the profile of the Fermi seas projected onto the p_z-p_t plane ($p_t=\sqrt{p_x^2+p_y^2}$) for the cases of (a) $U_A<m$, (b) $U_A>m$ and (c) $m=0$. As is already mentioned these seas still hold the axial symmetry around the z-axis and the reflection symmetry with respect to the p_x-p_y plane. The region surrounded by the outer line show the Fermi sea of "spin"-down quarks, and the shaded region is that of "spin"-up quarks.

We can see in Fig. 1(a) that the Fermi seas for the "spin"-down and "spin"-up states are deformed in the prolate and oblate shapes, respectively, where the minimum of the single-particle energy still resides at the origin $\boldsymbol{p}=0$. When $U_A>m$ as shown in Fig. 1(b), there appear two minima at the points $(p_t,p_z)=(0,\pm\sqrt{U_A^2-m^2})$ for the "spin"-down quark. Hence in the massless limit, $m\to 0$, the Fermi sea is described by two identical spheres with radii μ in the momentum space, which are centered at the points $(p_t,p_z)=(0,\pm U_A)$ [see Fig. 1(c)].

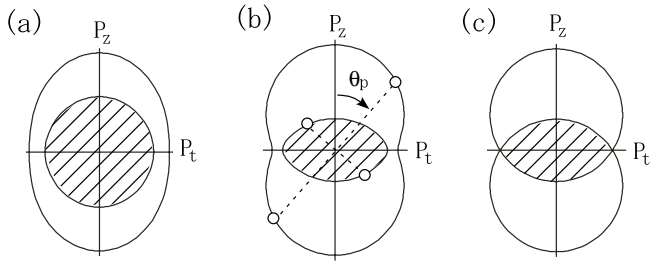

FIG. 1. Illustrations of the Fermi surfaces in the p_t-p_z plane with $p_t\equiv\sqrt{p_x^2+p_y^2}$. (a) For $\mu>U_A+m$ and $U_A\leqslant m$. Outer closed curve corresponds to the Fermi surface of the "spin"-down state with single-particle energy $\epsilon_-(\boldsymbol{p})$ and inner one surrounding the shaded area to the "spin"-up state with $\epsilon_+(\boldsymbol{p})$. (b) The same for (a) but $U_A\geqslant m$. A pair of white circles connected by a dashed line represents the Cooper pair characterized by B_n (27). Each particle in the Cooper pair has a different color and flavor. (c) The Fermi surfaces for $m\to 0$. The outer (inner) contour represents the Fermi surface for ϵ_- (ϵ_+).

In what follows we use subscript n ($=1,2,3,4$) for notational convenience as ϵ_n which means $\{\epsilon_1,\epsilon_2,\epsilon_3,\epsilon_4\}=\{\epsilon_-,\epsilon_+,-\epsilon_-,-\epsilon_+\}$. We define the spinor $\phi_n(\boldsymbol{p})$ that satisfies the equation $G_A^{-1}(p_0=\epsilon_n-\mu)\phi_n(\boldsymbol{p})=0$, which corresponds to the eigenspinor with the single-particle energy ϵ_n in the absence of the quark Cooper pairing. The spinor $\phi_n(\boldsymbol{p})$ is explicitly given as

$$\phi_n(\boldsymbol{p})=\mathcal{N}_n\begin{pmatrix}[\epsilon_n-(-1)^n\beta_p-U_A](p_x-ip_y)p_z\\ -[(-1)^n\beta_p+m]p_t^2\\ \{-[(-1)^n\beta_p+m](\epsilon_n-m-U_A)+p_z^2\}(p_x-ip_y)\\ p_t^2p_z\end{pmatrix}, \tag{23}$$

where

$$\mathcal{N}_n=\sqrt{[\beta_p-(-1)^nm][\epsilon_n+U_A+(-1)^n\beta_p]/(\epsilon_n\beta_p)}/(2p_t^2p_z)$$

and $\beta_p\equiv\sqrt{p_z^2+m^2}$. It is to be noted that the spinors ϕ_n do not return to the spinors of free quark even when $U_A\to 0$, but become mixtures of them, see Appendix A. Introducing the projection operator $\Lambda_n=\phi_n\phi_n^\dagger$ with properties $\Lambda_m\Lambda_n=\Lambda_n\delta_{mn}$ and $\Sigma_n\Lambda_n=\mathbf{1}$, we can recast $G_A(p)$ in the spectral representation into

$$G_A=\sum_n\frac{\Lambda_n}{p_0-\epsilon_n+\mu}\gamma_0 \tag{24}$$

$$G_A^{-1}=\sum_n(p_0-\epsilon_n+\mu)\gamma_0\Lambda_n. \tag{25}$$

B. Gap structure

In this subsection, we give the explicit form of the gap function Δ in the Dirac, color, and flavor spaces, and then calculate the diagonal component of the full Green function $G_{11}(p)$ in Eq. (7), provided that only the axial-vector self-energy is taken for $V(p)$ in Eq. (14). In general various types of the gap structures are possible in the Dirac, color, and flavor spaces; they depend on the form of interaction and the quark mass [2,19], especially on the strange quark mass [20].

Here we suppose a simple gap structure from a physical consideration, disregarding the finite mass effect.

Using the spinor $\phi_n(\boldsymbol{p})$ we assume that the gap function Δ in Eq. (15) has the following form in the color and flavor spaces:

$$\Delta(\boldsymbol{p}) = \sum_n \tilde{\Delta}_n(\boldsymbol{p}) B_n(\boldsymbol{p}) \tag{26}$$

with the operator $B_n(\boldsymbol{p})$,

$$B_n(\boldsymbol{p}) = \gamma_0 \phi_{-n}(\boldsymbol{p}) \phi_n^\dagger(\boldsymbol{p}), \tag{27}$$

where the subscript $-n$ $(=-1,-2,-3,-4)$ indicates that the single-particle energy in the spinor is replaced by that of opposite sign, $\epsilon_{-n} \equiv -\epsilon_n$, without change of "spin."

One can easily see what kind of quark pairs the gap function Δ (26) represents. Utilizing the property, $\phi_{-n'}^T(-\boldsymbol{p}) C \gamma_0 \phi_n(\boldsymbol{p}) \propto \delta_{n'n}$, one can find for the general spinor $\psi(\boldsymbol{p}) = \Sigma_n a_n(\boldsymbol{p}) \phi_n(\boldsymbol{p})$ with arbitrary coefficients a_n,

$$\overline{\psi}_c B_n \psi = \psi^T(-p) C \gamma_0 \phi_{-n} \phi_n^\dagger \psi(p) \propto a_n(-\boldsymbol{p}) a_n(\boldsymbol{p}). \tag{28}$$

This equation clearly shows that two quarks included in the Cooper pairing have opposite momenta to each other and belong to the same energy eigenstate as illustrated in Fig. 1(b).

Now we should note that the antisymmetric nature of the fermion self-energy imposes a constraint on the gap function [2,21],

$$C \Delta(\boldsymbol{p}) C^{-1} = \Delta^T(-\boldsymbol{p}). \tag{29}$$

Since B_n satisfies the relation $C B_n(\boldsymbol{p}) C^{-1} = B_n^T(-\boldsymbol{p})$, $\tilde{\Delta}_n(\boldsymbol{p})$ must be a symmetric matrix in the spaces of internal degrees of freedom. Taking into account the property that the most attractive channel of the OGE interaction is the color antisymmetric **3*** one, it must be the flavor singlet state. Thus we can choose the form of the gap function as

$$[\tilde{\Delta}_n(\boldsymbol{p})]_{\alpha\beta,\ ij} = \epsilon_{\alpha\beta 3} \epsilon_{ij} \Delta_n(\boldsymbol{p}), \tag{30}$$

where $(\alpha\beta)$ and (ij) are indices in three-color and two-flavor spaces, respectively. The form of gap function (30) in the color and flavor spaces is familiar for two-flavor CSC [2,3].

Using the properties of $\Lambda_n(\boldsymbol{p})$ and $B_n(\boldsymbol{p})$, we then obtain an explicit form of $G_{11}(p)$ as

$$\begin{aligned}
&[G_{11}(p)]_{\alpha\beta,ij} \\
&= \left\{ \sum_n \left[(p_0 + \mu - \epsilon_n) - \frac{\tilde{\Delta}_n^\dagger \tilde{\Delta}_n}{p_0 + \epsilon_n - \mu} \right] \gamma_0 \Lambda_n \right\}^{-1}_{\alpha\beta,ij} \\
&= \sum_n \frac{p_0 - \mu + \epsilon_n}{p_0^2 - (\epsilon_n - \mu)^2 - |\Delta_n|^2 (1 - \delta_{3\alpha}) + i\eta} \Lambda_n \gamma_0 \delta_{\alpha\beta} \delta_{ij}
\end{aligned} \tag{31}$$

with

$$\tilde{\Delta}_n^\dagger \tilde{\Delta}_n = \mathrm{diag}(|\Delta_n|^2,\ |\Delta_n|^2,\ 0) \ \text{ in the color space,} \tag{32}$$

where η is a positive infinitesimal.

The quasiparticle energies are obtained by looking for the poles of $G_{11}(p)$,

$$E_n(\boldsymbol{p}) = \begin{cases} \sqrt{(\epsilon_n(\boldsymbol{p}) - \mu)^2 + |\Delta_n(\boldsymbol{p})|^2} & \text{for color 1, 2} \\ \sqrt{(\epsilon_n(\boldsymbol{p}) - \mu)^2} & \text{for color 3.} \end{cases} \tag{33}$$

The quark number density ρ_q is also given as

$$\rho_q \equiv -i \int \frac{\mathrm{d}^4 p}{(2\pi)^4} \mathrm{Tr}\{[G_{11}(p) - G_{11}(p)|_{\mu=0}] \gamma_0\} \tag{34}$$

$$\begin{aligned}
&= N_f \sum_{n=1,2} \int \frac{\mathrm{d}^3 p}{(2\pi)^3} \{\theta(\mu - \epsilon_n) \\
&\quad + 2 v_n^2(\boldsymbol{p}) - 2[1 - v_{-n}^2(\boldsymbol{p})]\}
\end{aligned} \tag{35}$$

with

$$v_n^2(\boldsymbol{p}) = \frac{1}{2} \left(1 - \frac{\epsilon_n(\boldsymbol{p}) - \mu}{E_n(\boldsymbol{p})} \right), \tag{36}$$

where the first two terms in Eq. (35) show the quark contributions, while the last term the antiquark contribution; $v_n^2(\boldsymbol{p})$ is the occupation probability of the quark pairs with momentum $\boldsymbol{p}$ and represents diffuseness of the momentum distribution.

Similarly we can know the self-consistent solutions satisfy our ansatz about the mean fields in V. From the above solutions we can easily obtain that $\mathrm{Tr}[G_{11}(p) i\gamma_5] = 0$, $\mathrm{Tr}[G_{11}(p)\gamma_i] \propto p_i$, $\mathrm{Tr}[G_{11}(p)\gamma_5\gamma_0] \propto p_z$ and $\mathrm{Tr}[G_{11}(p)\gamma_5\gamma_{1,2}] \propto p_x, p_y$. Hence the pseudoscalar mean field U_{ps}, the space-component of vector mean field U_v^i, the axial-vector mean fields U_{av}^0 and $U_{av}^{1,2}$ are vanished after the integration over angles.

C. Equation for the superconducting gap function

Using Eq. (31), the off-diagonal component of the full Green function $G(p)$, given in Eq. (8), can be represented in the similar way as

$$G_{21}(p) = -\sum_n \frac{\gamma_0 B_n \gamma_0}{p_0^2 - (\epsilon_n - \mu)^2 - |\Delta_n|^2 + i\eta} \Delta_n \lambda_2 \tau_2, \tag{37}$$

where τ_2 is the Pauli matrix in the two-flavor space. Substituting Eq. (37) into the gap equation (15) and using the identity $\Sigma_{a=1}^8 (\lambda_a)^T \lambda_2 \lambda_a = -8/3 \lambda_2$, we obtain

$$\sum_{n'} B_{n'}(\boldsymbol{k})\Delta_{n'}(\boldsymbol{k}) = -i\frac{2}{3}g^2\int \frac{\mathrm{d}^4p}{(2\pi)^4}D_{\mu\nu}(k-p) \times\sum_n \left[\frac{\gamma^\mu\gamma_0 B_n(\boldsymbol{p})\gamma_0\gamma^\nu}{p_0^2-(\epsilon_n-\mu)^2-|\Delta_n|^2+i\eta}\right]\Delta_n(\boldsymbol{p}), \tag{38}$$

where the factor 2/3 is simply the Fierz coefficient for the color and flavor degrees of freedom (Appendix D). Furthermore multiplying both sides of Eq. (38) by $B^\dagger_{n'}(\boldsymbol{k})$ and taking trace with respect to the Dirac indices, the coupled equations for the gap functions Δ_n are obtained after p_0 integration,

$$\Delta_{n'}(\boldsymbol{k}) = -\frac{2}{3}g^2\int \frac{\mathrm{d}^3p}{(2\pi)^3}D_{\mu\nu}(k-p)\sum_n T^{\mu\nu}_{n'n}(\boldsymbol{k},\boldsymbol{p})\frac{\Delta_n(\boldsymbol{p})}{2E_n(\boldsymbol{p})}, \tag{39}$$

where the function $T^{\mu\nu}_{n'n}(\boldsymbol{k},\boldsymbol{p})$ is defined as

$$T^{\mu\nu}_{n'n}(\boldsymbol{k},\boldsymbol{p}) \equiv \mathrm{Tr}[B^\dagger_{n'}(\boldsymbol{k})\gamma^\mu\gamma_0 B_n(\boldsymbol{p})\gamma_0\gamma^\nu] = [\overline{\phi}_{-n'}(\boldsymbol{k})\gamma^\mu\phi_{-n}(\boldsymbol{p})][\overline{\phi}_n(\boldsymbol{p})\gamma^\nu\phi_{n'}(\boldsymbol{k})], \tag{40}$$

a decomposition of $B_n(\boldsymbol{p})$ in terms of gamma matrices and its properties are given in Appendix B.

Here we take the zero-range approximation in Eq. (17). In terms of the polar coordinates $\boldsymbol{p}=\{p,\theta_p,\phi_p\}$, we can consider that the gap function $\Delta_n(\boldsymbol{p})$ does not depend on the horizontal angle ϕ_p due to axial-symmetry around the p_z axis. Thus we can explicitly perform the integration with respect to the angle ϕ_p in the gap equation (39),

$$\Delta_{n'}(k,\theta_k) = \frac{2}{3}\tilde{g}^2\int \frac{\mathrm{d}p\,\mathrm{d}\theta_p}{(2\pi)^2}p^2\sin\theta_p \times\sum_n T_{n'n}(k,\theta_k,p,\theta_p)\frac{\Delta_n(p,\theta_p)}{2E_n(p,\theta_p)} \tag{41}$$

with the effective coupling constant $\tilde{g}\equiv g/\sqrt{Q^2+M^2}$. As seen from the above equation, each of the gap functions couples with others by the function $T_{n'n}(k,\theta_k,p,\theta_p)$ defined as

$$T_{n'n}(k,\theta_k,p,\theta_p) \equiv \int\frac{\mathrm{d}\phi_p}{2\pi}g_{\mu\nu}T^{\mu\nu}_{n'n}(\boldsymbol{k},\boldsymbol{p}) = \frac{k_t p_t}{2|\epsilon_{n'}(\boldsymbol{k})||\epsilon_n(\boldsymbol{p})|} \times\left[(-1)^{n'+n}\frac{2m^2+k_z p_z}{\beta_p\beta_k}+1\right], \tag{42}$$

where $p_t\equiv p\sin\theta_p$ and $p_z\equiv p\cos\theta_p$ and the same for k_t and k_z. The term proportional to p_z in Eq. (42) will disappear after the integration over θ_p.

D. Equation for the axial-vector mean-field U_A

Using Eqs. (33) and (36), $G_{11}(p)$ is recasted in the form

$$[G_{11}(p)]_{\alpha\beta,\ ij} = \left[\sum_n\left(\frac{1-v_n^2(\boldsymbol{p})}{p_0-E_n+i\eta}+\frac{v_n^2(\boldsymbol{p})}{p_0+E_n-i\eta}\right) \times e^{ip_0\eta}\Lambda_n(\boldsymbol{p})\gamma_0\right]\delta_{\alpha\beta}\delta_{ij}. \tag{43}$$

Substituting the above equation into Eq. (14), and integrating with respect to p_0, we obtain the self-consistent equation for U_A in the zero-range approximation,

$$U_A = -\frac{2}{9}\frac{N_f}{2}\tilde{g}^2\int\frac{\mathrm{d}^3p}{(2\pi)^3} \times\sum_n[\theta(\mu-\epsilon_n(\boldsymbol{p}))+2v_n^2(\boldsymbol{p})]S_n(\boldsymbol{p}), \tag{44}$$

where the factor $-2/9$ stems from the Fierz coefficient of the color-singlet axial-vector channel of the OGE interaction (Appendix D), and $S_n(\boldsymbol{p})$ is the expectation value of the spin operator, $\sigma_z\equiv-\gamma_0\gamma_5\gamma_3$, with respect to the spinor $\phi_n(\boldsymbol{p})$:

$$S_n(\boldsymbol{p}) \equiv \mathrm{Tr}(\gamma_5\gamma_3\Lambda_n(\boldsymbol{p})\gamma_0) = \phi_n^\dagger(\boldsymbol{p})(-\sigma_z)\phi_n(\boldsymbol{p}) = \frac{U_A+(-1)^n\beta_p}{\epsilon_n(\boldsymbol{p})}. \tag{45}$$

Thus U_A is related to the expectation value of σ_z summing over the state with momentum $\boldsymbol{p}$. An effect of the Cooper pairing enters into Eq. (44) through the function $v_n(\boldsymbol{p})$.

E. Weak coupling approximation

In this subsection we consider a high-density limit, which means the weak coupling limit due to asymptotic freedom of QCD, and then disregards the antiquark pairing and contributions from the negative-energy sea (the Dirac sea) in Eq. (41). Actually it costs more energy to form the anti-quark pairing than the quark pairing for a large chemical potential. Taking the approximation, we also disregard the contribution from anti-quarks to calculate the quark number density in Eq. (35) and the axial-vector mean-field Eq. (44) consistently.[2] In the following calculations we define gap functions of the quark pairing by subscript $\pm$ which corresponds to the ''spin''-up (-down) of positive-energy states as $\Delta_-\equiv\Delta_1$ and $\Delta_+\equiv\Delta_2$. The other symbols with the subscript $\pm$ have the same meaning, e.g., $\phi_\mp\equiv\phi_{1,2}$.

In addition, we assume that only quarks near the Fermi surface form the Cooper pairs, and thereby replace the gap function by an approximated form,

[2]This is equivalent to the restriction of the sum over the index $n(n=1-4)$ to 1,2, which correspond to the positive-energy states with different ''spins'' specified by the subscript $\mp$.

$$\Delta_\pm(\boldsymbol{p}) \to \Delta_\pm(\boldsymbol{p})\,\theta(\delta - |\epsilon_\pm - \mu|), \tag{46}$$

where δ is a cutoff parameter around the Fermi surface. The function $\theta(\delta - |\epsilon_\pm(\boldsymbol{p}) - \mu|)$ is also regarded as a form factor to regularize the integration in the gap equation [21]. The step-function form factor mimics the asymptotic freedom; inner particles in Fermi sea costs large kinetic energy to create the pairing and takes large momentum transfer which indicates that coupling of this inner process is small. There, however, might be more realistic form factors for finite density QCD, which are smoother functions of momentum and μ than ours, we think that they makes little change on qualitative results of the CSC and spin polarization. There are models with other form factors or cut-off functions [3,5].

Looking at the structure of the gap equation (41) with (42), one can find that the gap function is exactly parametrized as (Appendix C)

$$\Delta_\pm(\boldsymbol{p}) = \frac{p_t}{\epsilon_\pm(\boldsymbol{p})}\left(\mp\frac{m}{\beta_p}R + F\right) \equiv \frac{p_t}{\epsilon_\pm(\boldsymbol{p})}\hat{\Delta}_\pm(\boldsymbol{p}), \tag{47}$$

where R and F are some constants and represent the antisymmetric and symmetric combinations of the gap functions; $2R = \beta_p/m(\hat{\Delta}_- - \hat{\Delta}_+) = \beta_p/(p_t m)(\epsilon_-\Delta_- - \epsilon_+\Delta_+)$ and $2F = \hat{\Delta}_- + \hat{\Delta}_+ = 1/p_t(\epsilon_-\Delta_- + \epsilon_+\Delta_+)$. Their magnitudes are determined by the coupled equations,

$$F = \frac{2}{3}\tilde{g}^2\int \frac{\mathrm{d}p\,\mathrm{d}\theta_p}{(2\pi)^2}p^2\sin\theta_p\frac{1}{4}\left[Q_+(\boldsymbol{p})\left(F - \frac{m}{\beta_p}R\right) + Q_-(\boldsymbol{p})\left(F + \frac{m}{\beta_p}R\right)\right] \tag{48}$$

$$R = \frac{2}{3}\tilde{g}^2\int \frac{\mathrm{d}p\,\mathrm{d}\theta_p}{(2\pi)^2}p^2\sin\theta_p\frac{m}{2\beta_p}\left[-Q_+(\boldsymbol{p})\left(F - \frac{m}{\beta_p}R\right) + Q_-(\boldsymbol{p})\left(F + \frac{m}{\beta_p}R\right)\right], \tag{49}$$

where

$$Q_\pm(\boldsymbol{p}) = \frac{p_t^2}{\epsilon_\pm(\boldsymbol{p})^2 E_\pm(\boldsymbol{p})}\,\theta(\delta - |\epsilon_\pm(\boldsymbol{p}) - \mu|).$$

We can obviously see that $R \to 0$ as $m \to 0$.

Here we examine the polar-angle dependence of the anisotropic gap function at the Fermi surface $\Delta_\pm(p^F, \theta)$. The Fermi momentum $p^F(\theta)$ of each ''spin'' eigenstate is given as

$$p_t = p_\pm^F(\theta)\sin\theta, \quad p_z = p_\pm^F(\theta)\cos\theta$$

with

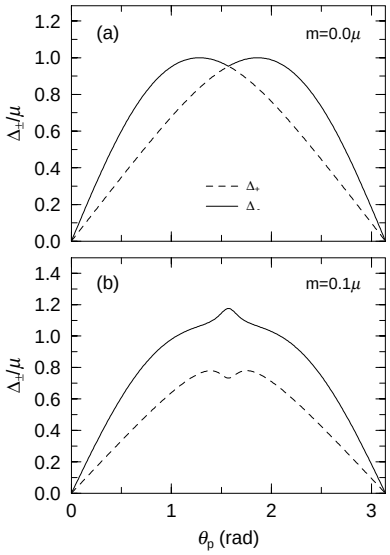

FIG. 2. A schematic view of polar-angle dependence of the gap functions at the Fermi surface where we set values of the gap parameters as $R = 0.2\mu$, $F = \mu$, $U_A = 0.3\mu$, (a) for $m = 0$ and (b) for $m = 0.1\mu$.

$$p_\pm^F(\theta) = [\mu^2 - m^2 + U_A^2\cos(2\theta) \mp U_A\sqrt{4\mu^2\cos^2\theta + 4m^2\sin^2\theta - U_A^2\sin^2(2\theta)}]^{1/2}, \tag{50}$$

where the subscript $\pm$ corresponds to the ''spin''-up (-down) state again. Substituting the above formula into the gap function (47), we get

$$\Delta_\pm(p_\pm^F, \theta) = \frac{p_\pm^F(\theta)\sin\theta}{\mu}\left[\mp\frac{m}{\sqrt{m^2 + [p_\pm^F(\theta)\cos\theta]^2}}R + F\right]. \tag{51}$$

Note that this form exhibits a *P*-wave pairing nature: it is a genuine relativistic effect by the Dirac spinors (Appendix B). We show a schematic view of the above gap functions in Fig. 2. As characteristic features, both the gap functions vanish at poles ($\theta = 0, \pi$) and take maximal values near equator ($\theta = \pi/2$), keeping the relation, $\Delta_- \geqslant \Delta_+$.[3] Suppression of Δ_+ and enhancement of Δ_- at $\theta = \pi/2$ for the case of $m \neq 0$ [Fig. 2(b)] are originated from a finite value of R, while they vanish if quark is taken to be massless [Fig. 2(a)]. The anisotropic gap functions give rise to the different diffuseness in the momentum distribution of the two ''spin'' eigenstates, and thereby make some effects on spin polarization, unlike in the normal phase. The anisotropic diffuseness has two effects that it obscures the deformation in the momentum distribution due to their angle dependence and enlarges the difference of the state density between the two ''spin'' eigenstates through the relation $\Delta_- \geqslant \Delta_+$.

[3]This feature is very similar to ^3P pairing in liquid ^{3}He [22] or nuclear matter [23].

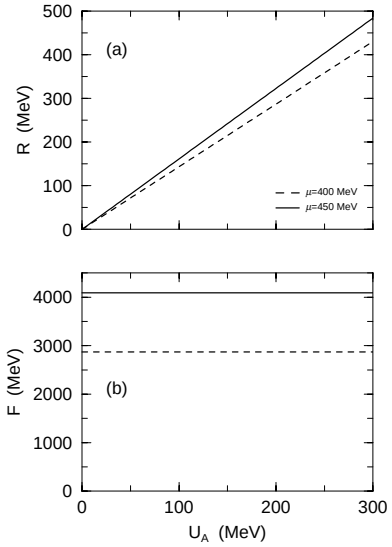

FIG. 3. Parameter dependence of R and F on U_A for $\tilde{g}=0.13\ \mathrm{MeV}^{-1}$, $m=20$ MeV, and $\delta=0.1\mu$. (a) For R and (b) for F. Dashed (solid) lines correspond to $\mu=400(450)$ MeV. The magnitudes of R and F are calculated by Eqs. (49) and (48) for given U_A.

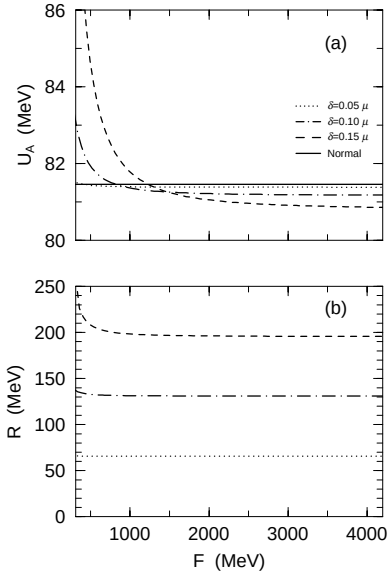

FIG. 4. Parameter dependence of U_A and R on F for $\tilde{g}=0.13\ \mathrm{MeV}^{-1}$, $m=20$ MeV, and $\mu=450$ MeV. (a) For U_A and (b) for R. Solid line, dotted lines, dot-dashed lines, and dashed lines correspond to $\delta=0$ (normal phase), 0.05μ, 0.10μ, and 0.15μ, respectively. The magnitudes of U_A and R are obtained by their equations for given F.

III. RESULTS AND DISCUSSIONS

In this section we solve the coupled Equations (44), (48), and (49) and investigate the effects of the superconducting gap on spin polarization.

Before going to numerical calculations of U_A, R, and F, each of which is coupled with others by the self-consistent equations, it is instructive to see their parameter dependence by treating one of them as an input parameter. First we show R and F as functions of U_A in Fig. 3 where $\mu=400,450$ MeV and $\delta=0.1\mu$. R starts from zero and almost linearly increases with U_A [Fig. 3(a)], which is understood by seeing that R is proportional to the difference, $\hat{\Delta}_- - \hat{\Delta}_+$, due to finite U_A, see Eq. (47) or Appendix C. Thus R is induced by U_A and closely coupled with it.

As for the behavior of F, it is barely affected by U_A (slight decreasing with U_A in the numerical value) [Fig. 3(b)]. As seen from the dependence on μ the magnitude of F is almost determined by the volume of the phase space in the gap equation, that is, by μ and δ. This reflects the fact that F is related to the sum, $\hat{\Delta}_+ + \hat{\Delta}_-$ (Appendix C). Thus we expect that F increases with density when other parameters are fixed.

From the above results we have found that F is not so much influenced by U_A. Next we examine the behavior of U_A and R when F is treated to be an input parameter. In Fig. 4 we show the parameter dependence of U_A and R on F, where $\mu=450$ MeV and we use three values of the cut off parameter $\delta=0.05\mu$, 0.1μ and 0.15μ, and add the result of U_A in the normal phase ($\delta=0$). Comparing the dependence of U_A on F [Fig. 4(a)] with that in the normal phase, we see a characteristic behavior for different values of δ: there are regions where U_A is larger than that in the normal phase for relatively small F, and this region seems to extend with δ. On the other hand results from the self-consistent calculations show that F becomes larger with δ so that its value corresponds to a region where U_A is comparable with or slightly less than that in the normal phase, for any value of the chemical potential. This situation seems to be qualitatively unchanged, once the ratio of the effective coupling constants in the axial-vector channel G_{axial} and the diquark channel G_{diq} is kept, $G_{axial}:G_{diq}=2/9:2/3$, which comes from the Fierz transformation for color and flavor (Appendix D). However, if the coupling constant in each channel is taken independently, our results might be changed qualitatively.

Seeing the results for R in Fig. 4(b), we find that R increases with δ due to the growth of the phase space and is hardly affected by F except the region of small F where U_A varies rapidly as shown in Fig. 4(a): it also shows that R is closely related to U_A.

These parameter dependences also suggest that the regularization scheme for the gap equation, i.e.,the sharp momentum cut-off function, the form factor, etc., will give rise to a qualitative change to U_A. In the present cut-off function, $\theta(\delta-|\epsilon_\pm-\mu|)$, U_A (spin polarization) coexists with CSC, except a slight competition, as will be shown later.

A. Self-consistent solutions

We demonstrate some self-consistent solutions here. Since we have little information to determine the values of the parameters $\tilde{g}$ and δ (there may be other more reasonable form factors than the present cutoff function), and our purpose is to figure out qualitative properties of spin polarization in the color superconducting phase, we mainly set in the

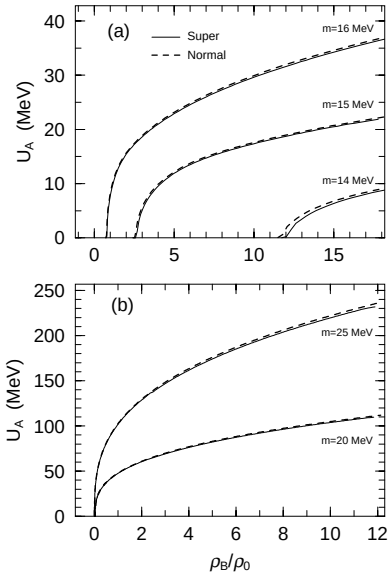

FIG. 5. Axial-vector mean field as a function of baryon number density ρ_B ($\rho_0 = 0.16$ fm^{-3}) for $\tilde{g} = 0.13$ MeV^{-1} and $\delta = 0.1\mu$. (a) For $m = 14 \sim 16$ MeV and (b) For $m = 20$ and 25 MeV. Dashed (solid) lines are obtained in the normal (color superconducting) phase.

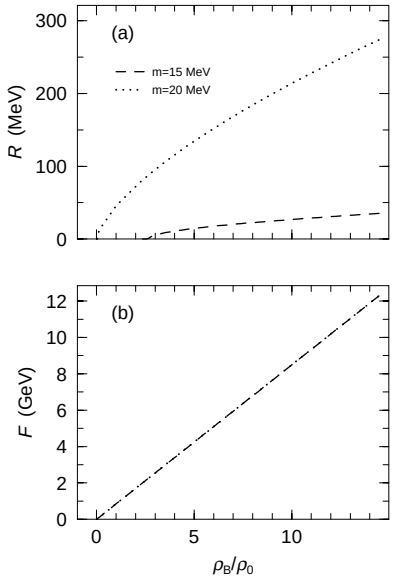

FIG. 6. R (a) or F (b) as a function of ρ_B/ρ_0 for $m = 15$ MeV (dashed lines) and $m = 20$ MeV (dotted lines). The other parameters are the same as in Fig. 5. Note that in (b) the lines almost overlap each other for the two quark masses.

following calculations them as $\tilde{g} = 0.13$ MeV^{-1} and $\delta = 0.1\mu$, for example, which is not so far from the couplings in NJL-like models [5,16,18].

We first examine spin polarization in the absence of CSC. In Fig. 5 we show the axial-vector mean-field U_A, with $\Delta_\pm$ being set to be zero, as a function of baryon number density $\rho_B (\equiv \rho_q/3)$ relative to the normal nuclear density $\rho_0 = 0.16$ fm^{-3} for $m = 14 \sim 25$ MeV (dashed lines). It is seen that the axial-vector mean field (spin polarization) appears above a critical density and becomes larger as baryon number density gets higher. Moreover, the results for different values of the quark mass show that spin polarization grows more for the larger quark mass. This is because a large quark mass gives rise to much difference in the Fermi seas of two opposite ''spin'' states, which leads to growth of the exchange energy in the axial-vector channel.

Next we solve the coupled equations (44), (48), and (49). Results for U_A, R, and F are shown in Fig. 5 (solid lines) and Fig. 6, for values of the quark mass $m = 14$–25 MeV. It is found again, by comparing these cases of the quark mass, that U_A is very sensitive to the quark mass and increases with it as in the absence of CSC (Fig. 5). For the behavior of the gap functions, R is induced by U_A and both of F and R increase with ρ_B due to the growth of the Fermi surface (Fig. 6). It is also seen that F is not sensitive to the quark mass. To see the bulk behavior of pairing gap as a function of baryon number density, we also show, in Fig. 7, their mean values with respect to the polar angle on the Fermi surface,

$$\langle \Delta_\pm \rangle \equiv \left(\int_0^\pi d\theta \frac{\sin\theta}{2} \Delta_\pm^2 \right)^{1/2}. \tag{52}$$

The mean values $\langle \Delta_\pm \rangle$ begin to split with each other at a density where U_A becomes finite. This reflects that R is induced by U_A and then has a negative (positive) contribution to Δ_+ (Δ_-). Here we would like to comment on the magnitude of $\langle \Delta_\pm \rangle$. These should be compared with the usual uniform gap function, and may look very large values of $O(\mathrm{GeV})$ in our case. However these values would be largely reduced by taking a smooth form factor which models asymptotic freedom of QCD [5]; it further reduces the integral value in the gap equation, compared with our sharp cutoff function.

In Fig. 8 we show the expectation value of the spin operator per quark, $\langle \sigma_z/N_q \rangle$, as a function of ρ_B/ρ_0 with and without the superconducting gap. The critical density becomes lower as the quark mass increases, and the peak positions of $\langle \sigma_z/N_q \rangle$ are located at relatively lower densities in each quark mass. The magnitude of $\langle \sigma_z/N_q \rangle$ is to be compared with 1 for a free quark, because $|\psi_s^\dagger \sigma_z \psi_s / \psi_s^\dagger \psi_s| = 1$ at the rest frame for the free spinor ψ_s. We arrange the results

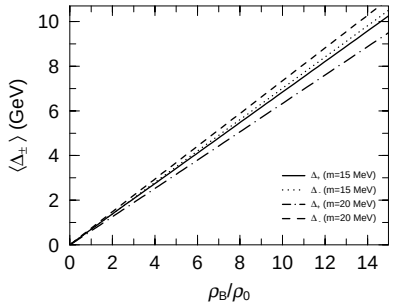

FIG. 7. Mean values of the gap functions with respect to the solid angle at the Fermi surface, $\langle \Delta_\pm \rangle$, plotted as a function of ρ_B/ρ_0 for $m = 15$ MeV (solid and dotted lines) and 20 MeV (dot-dashed and dashed lines).

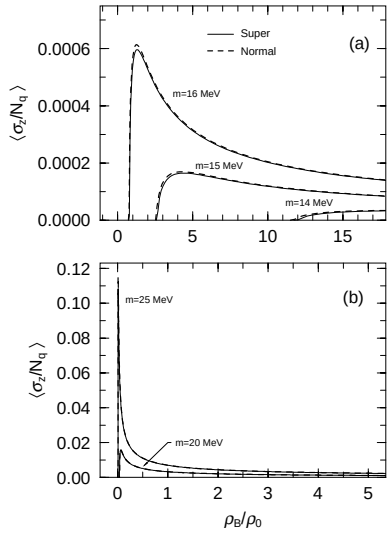

FIG. 8. Spin expectation value per quark as a function of ρ_B/ρ_0. (a) For $m=14$–16 MeV and (b) $m=20$ and 25 MeV. Dashed (solid) lines show results in the normal (color superconducting) phase.

of three quark masses $m=14\sim16$ MeV by 1 MeV in Fig. 8(a) to show a high sensitivity of spin polarization to the quark mass, which implies that the exchange energy from the attractive axial-vector interaction is strongly enhanced by the quark mass to produce the large axial-vector mean-field. The exchange energy is also enhanced by larger chemical potential and the resulting axial-vector mean-field increases with it (see Fig. 5). But the spin expectation value per quark, which is relative to the axial-vector mean-field per quark ($\propto U_A/N_q$), has an upper limit since the increase of N_q is far superior to that of U_A for larger chemical potential, which gives rise to the peak positions in Fig. 8.

The quark mass is very important in relation to the breaking of chiral symmetry in QCD. Models incorporating chiral dynamics have indicated that the dynamical mass becomes smaller as chiral symmetry is restored at a high density, while the current quark mass is small and explicitly breaks it [24]. In our model, on the other hand, we treat the quark mass m as a variable parameter so that we may simulate a change of the dynamical mass. In order to further examine the effect of the quark mass on spin polarization, we show the mass dependence at densities $\rho_B=5\rho_0$, $\rho_B=10\rho_0$ and $\rho_B=15\rho_0$ for the cases with and without the superconducting gap in Fig. 9. Spin polarization increases with the quark mass in all the three densities. In the figure we exhibit only the results for a narrow region of the mass parameter ($m=13\sim20$ MeV), while as for larger masses of $O(100$ MeV) (order of the strange quark mass) spin polarization monotonically increases without singular oscillations. Critical values of the quark mass at which spin polarization disappears become smaller as density increases in both cases.

In relation of U_A to m we can derive an exact result in the massless limit, $m\to0$. In the normal phase where $\Delta=0$, Eq. (44) becomes

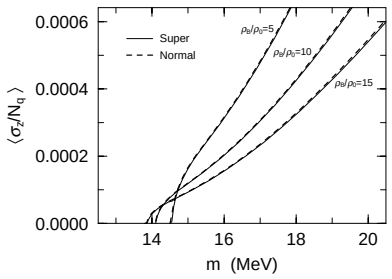

FIG. 9. Spin expectation value per quark as a function of the quark mass m for fixed baryon number density $\rho_B/\rho_0=5$, 10, and 15.

$$U_A=-\frac{2}{9}\tilde{g}^2\sum_{n=1,2}\int\frac{d^3p}{(2\pi)^3}3\times\theta(\mu-\epsilon_n(\boldsymbol{p}))\frac{U_A+(-1)^n|p_z|}{\epsilon_n(\boldsymbol{p})} \tag{53}$$

with

$$\epsilon_\pm(\boldsymbol{p})=\sqrt{(|p_z|\pm U_A)^2+p_t^2}. \tag{54}$$

The right-hand side of the above equation can be analytically integrated to give

$$U_A=-\frac{2}{9}\tilde{g}^2\frac{4\pi}{(2\pi)^3}3\int_0^{\mu-U_A}dp_z\int_0^{\sqrt{\mu^2-(p_z+U_A)^2}}dp_tp_t\times\frac{U_A+p_z}{\sqrt{(p_z+U_A)^2+p_t^2}}-\frac{2}{9}\tilde{g}^2\frac{4\pi}{(2\pi)^3}3\int_0^{\mu+U_A}dp_z\times\int_0^{\sqrt{\mu^2-(p_z-U_A)^2}}dp_tp_t\frac{U_A-p_z}{\sqrt{(p_z-U_A)^2+p_t^2}}=0. \tag{55}$$

Here we have assumed that $\mu>U_A$. In the massless limit, the Fermi sea is described by two complete spheres in the momentum space with radii μ, whose centers are located at $(p_t,p_z)=(0,\pm U_A)$ [see Fig. 1(c)]. The momentum distribution for quarks in the ''spin''-down state occupies these two spheres, while the ''spin''-up state does their overlap region (shaded). In the above integration for the ''spin''-down quarks, the expectation value of the spin operator given by quarks with $0\leqslant p_z\leqslant U_A$ is canceled with that of quarks with $U_A\leqslant p_z\leqslant 2U_A$. The remaining contribution from the region, $2U_A\leqslant p_z\leqslant\mu+U_A$, cancels with that by the ''spin''-up quarks. Thus we can see that spin polarization disappears as $m\to0$ in the absence of CSC.

This analytical result that $U_A\to0$ as $m\to0$ can be also understood as follows. The eigenstates of non-interacting massless fermions are classified by the definite helicity states: the positive energy state is right-handed (left-handed) with positive (negative) helicity, while the negative energy state those with negative (positive) helicity. This property is not spoiled by introducing the axial-vector mean-field, when

we extend the meaning of helicity; the Dirac equations for the ''left-'' and ''right-handed'' positive-energy fermion fields $\psi_{L,R}$ are now given as

$$(p_0+\boldsymbol{p}\cdot\boldsymbol{\sigma}+U_A\sigma_3)\psi_L=0, \tag{56}$$

$$(p_0-\boldsymbol{p}\cdot\boldsymbol{\sigma}+U_A\sigma_3)\psi_R=0, \tag{57}$$

which give the eigenvalues,

$$p_0=\sqrt{p_t^2+(p_z+U_A)^2}[\equiv\epsilon_L(\boldsymbol{p})]$$

for ψ_L and $p_0=\sqrt{p_t^2+(p_z-U_A)^2}[\equiv\epsilon_R(\boldsymbol{p})]$ for ψ_R. ψ_L (ψ_R) is the eigenstate of generalized helicity $h=\mp 1$ projected onto the shifted momentum $\boldsymbol{p}'=\{p_x,p_y,p_z\pm U_A\}$. If $\mu\neq 0$ they form the spherical Fermi seas, see Fig. 1(c). Here it would be interesting to compare these eigenvalues with the limit form of $\epsilon_\pm(\boldsymbol{p})$ in Eq. (22),

$$\epsilon_\pm(\boldsymbol{p})\to\sqrt{p_t^2+(|p_z|\pm U_A)^2}\ \text{ as }\ m\to 0. \tag{58}$$

Then we can see the relations: $\epsilon_\pm(\boldsymbol{p})=\epsilon_L(\boldsymbol{p})\theta(\pm p_z)+\epsilon_R(\boldsymbol{p})\theta(\mp p_z)$, which clearly show that the two Fermi seas of the eigenspinors (23) give the same Fermi seas of $\psi_{L,R}$ for a given chemical potential μ. Thus we can take an alternative view of the Fermi seas in terms of the definite helicity states by rearranging the eigenspinor (23) properly in the massless limit. In each Fermi sea for $\psi_{L,R}$ the particle number with the definite h becomes the same, and thereby the total spin-expectation value becomes vanished.

In the color superconducting phase, on the other hand, the situation is different because the momentum distribution becomes diffused due to the creation of the Cooper pairs near the Fermi surface. For $m\to 0$ and $\Delta_\pm\neq 0$, Eq. (44) becomes

$$U_A=-\frac{2}{9}\tilde{g}^2\sum_{n=1,2}\int\frac{\mathrm{d}^3p}{(2\pi)^3}2v_n^2(\boldsymbol{p})\frac{U_A+(-1)^n|p_z|}{\epsilon_n(\boldsymbol{p})}, \tag{59}$$

where $v_n^2(\boldsymbol{p})$ indicates the diffused part of the momentum distribution, defined in Eq. (36). Here we should note that the gap functions $\Delta_\pm$ are still nonzero even at $m=0$. The diffused part, however, give no contribution to the spin polarization from the viewpoint of the helicity eigenstates. The gap function in the massless limit becomes

$$\Delta_\pm(p,\theta)=\frac{p_t}{\sqrt{(|p_z|\pm U_A)^2+p_t^2}}F, \tag{60}$$

see Fig. 2(a). The diffuseness from the above gap function has an equal contribution to the two complete Fermi spheres of chirality. Thus the total spin, which is obtained by summing up these momentum distributions, should be zero in the massless limit even if the CSC is taken into account.

To summarize we show a phase diagram for the quark mass and baryon number density in Fig. 10 where we add the result of $\tilde{g}=0.26\ \mathrm{MeV}^{-1}$ to see the dependence on the coupling constant. The lines indicate the critical mass at a fixed density (at regions above the lines spin polarization arises).

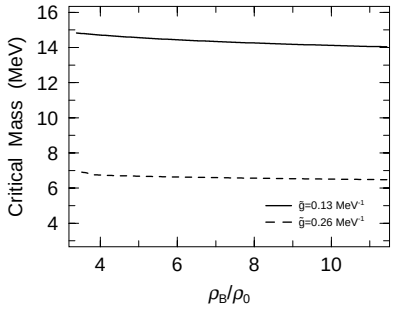

FIG. 10. Phase diagram in ρ_B/ρ_0-m plane for the effective coupling constant $\tilde{g}=0.13\ \mathrm{MeV}^{-1}$ and $0.26\ \mathrm{MeV}^{-1}$. At regions above the lines spin polarization arises. This result is obtained with the gap function, thus all the region in the phase diagram shows the color superconducting phase.

We can confirm that the critical mass becomes smaller with the increase of the density, and spin polarization occurs at moderate densities ($\rho_B=3\sim 4\rho_0$) if the coupling is strong enough even though quark mass is taken to be smaller as a simulation for change of dynamical mass (restoration of chiral symmetry).

Here we would like to understand how the gap function affects spin polarization and brings about a slight reduction of it. In the spin-polarized phase, the momentum distribution is deformed from the simple spherical shape. As mentioned in Ref. [13], the deformation is induced by finite U_A and feeds back to U_A in a self-consistent manner. In the color superconducting phase, diffuseness caused by the Cooper pairing in the momentum distribution depends on the polar angle and then has an influence on the deformation. As can be expected from the polar-angle dependence of the gap function, diffuseness tends to obscure the deformation.

From the consideration of the spin expectation values by spinors (23) near the Fermi surfaces;

$$\phi_\pm^\dagger(-\sigma_z)\phi_\pm=\frac{U_A\pm\sqrt{p_z^2+m^2}}{\epsilon_\pm}\approx\frac{U_A\pm\sqrt{p_z^2+m^2}}{\mu}, \tag{61}$$

where $\phi_\mp\equiv\phi_{1,2}$ for two ''spins.'' The difference of the spin expectation value between two ''spin'' states $\phi_\pm$ is largely affected by high-p_z regions or regions near both poles ($\theta=0,\pi$). Thus the large deformation along the z axis seems to enhance spin polarization.

In order to specify to what extent the Fermi sea is deformed, we calculate the quadrupole deformation of the momentum distribution defined by

$$Q_2\equiv 3\langle p_z^2\rangle/\langle\boldsymbol{p}^2\rangle-1. \tag{62}$$

In Fig. 11, we show Q_2 as a function of U_A at $\mu=450$ MeV in the normal phase and in the color superconducting phase in which the gap functions are given by their equations for fixed U_A. From this result of Q_2 deformation, we can see that the diffused part near the Fermi surface obscures the deformation then gives an opposite effect against Q_2, and thus reduces spin polarization.

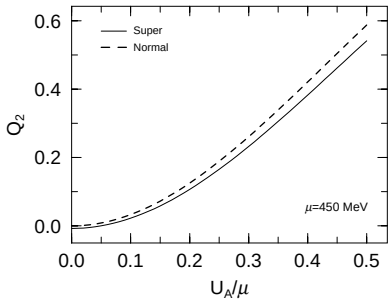

FIG. 11. Quadrupole deformation of the momentum distribution (62) as a function of U_A. Parameters are fixed as $\tilde{g}=0.13\ \mathrm{MeV}^{-1}$, $m=20$ MeV, and $\mu=450$ MeV. Dashed (solid) line is given in the normal (color superconducting) phase.

Nevertheless the gap function has another effect on spin polarization. It is to be noted that the qualitative relation, $\Delta_- \geqslant \Delta_+$, is always retained as seen from Fig. 2 and then has a effect to enlarge the difference of the state density between the two ''spin'' states. This effect is expected to enhance spin polarization since the difference of the spin expectation value by each spinor (61) near the equator ($\theta=\pi/2$), so that $p_z \approx 0$, seems to depend only on the difference of the state density. To see it in both the normal and color superconducting phases, we define that N_{up} (N_{down}) is the state density of the ''spin''-up (-down) state and show their difference by $dN \equiv N_{down}-N_{up}$, only in the first two colors, as a function of U_A in Fig. 12 at $\mu=450$ MeV. The result indicates that the gap functions slightly enhance dN than normal phase.

From the above discussions spin polarization is significantly influenced by both the deformation and the state density in each ''spin'' state. As a result of the self-consistent calculation in the color superconducting phase, the reduction effect on the deformation is slightly superior to the enhancement effect from the difference of the state densities, and the pairing effect finally reduces spin polarization than in the normal phase. It, however, should be noted that this qualitative conclusion about whether CSC enhances spin polarization than normal phase or not is very delicate and may be changed depending on the regularization scheme, as already mentioned. Moreover other types of pairing which are not considered here, e.g., pairing of the ''spin'' -up and -down states, may gives rise to qualitatively different results, while

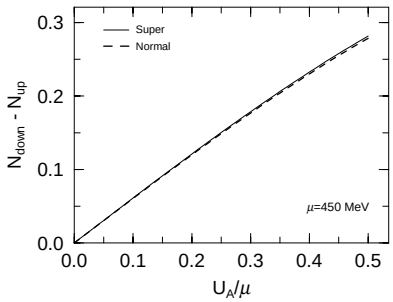

FIG. 12. Difference of the state densities in the two ''spin'' states plotted as a function of U_A. Legends are the same as in Fig. 11.

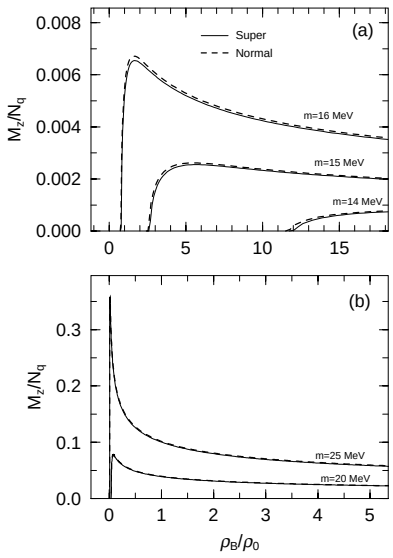

FIG. 13. Induced magnetic moment per quark (63) as a function of ρ_B/ρ_0. Parameters and legends are the same as in Fig. 5.

it is very difficult to see which type of pairing is energetically favored.

Finally we would like to comment on the coupling of the spin polarized quark matter with the external magnetic field; quark fields couple with the magnetic field through its anomalous magnetic moment. The magnetic interaction is described by the Gordon identity for the gauge coupling term: $g_L e^*/2m(\bar{\psi}\sigma_{\mu\nu}\psi)F^{\mu\nu}$ where g_L is a form factor and e^* an effective charge.[4] In quark matter a magnetic moment is given as the expectation value $\langle\sigma_{ij}\rangle$ with respect to the ground state. In our model only $\langle\sigma_{12}\rangle$ is nonzero, and the magnetic moment per quark is given as

$$M_z \equiv \langle \sigma_{12}/N_q \rangle = \frac{1}{\rho_q} \sum_{n=1,2} \int \frac{d^3p}{(2\pi)^3} [2v_n^2(\boldsymbol{p}) + \theta(\mu-\epsilon_n)]\bar{\phi}_n(\boldsymbol{p})\sigma_{12}\phi_n(\boldsymbol{p}). \tag{63}$$

Note that the expectation value of σ_{12} by the spinor does not depend on U_A; $\bar{\phi}_\pm(\boldsymbol{p})\sigma_{12}\phi_\pm(\boldsymbol{p}) = \mp m/\beta_p$, so that M_z reflects only the asymmetry in the momentum distribution due to the axial-vector mean-field. In Fig. 13, M_z is given as a function of baryon number density. This indicates that resulting ground state also holds ferromagnetism (spontaneous magnetization).

[4]Here we need not consider the orbital angular momentum for uniform matter. But if a superconductor is of the ''second'' type in which London's penetration length is larger than the coherence length, a vortex lattice may be formed in response to the external field and then total magnetization is to undergo a qualitative change due to circulation of supercurrent [25].

IV. SUMMARY AND CONCLUDING REMARKS

In this paper we have examined spin polarization in quark matter in the color superconducting phase. We have introduced the axial-vector self-energy and the quark pair field (the gap function), whose forms are derived from the one-gluon-exchange interaction by way of the Fierz transformation under the zero-range approximation. Within the relativistic Hartree-Fock framework we have evaluated their magnitudes in a self-consistent manner by way of the coupled Schwinger-Dyson equations.

As a result of numerical calculations spontaneous spin polarization occurs at a high density for a finite quark mass in the absence of CSC, while it never appears for massless quarks as an analytical result. In the spin-polarized phase the single-particle energies corresponding to spin degrees of freedom, which are degenerate in the noninteracting system, are split by the exchange energy in the axial-vector channel. Each Fermi sea of the single-particle energy deforms in a different way, which causes an asymmetry in the two Fermi seas and then induces the axial-vector mean-field in a self-consistent manner. In the superconducting phase, however, spin polarization is slightly reduced by the pairing effect; it is caused by competition between reduction of the deformation and enhancement of the difference in the phase spaces of opposite ''spin'' states due to the anisotropic diffuseness in the momentum distribution.

In connection of the deformation with superconductivity it has recently been reported [26] that in the superconducting asymmetric nuclear matter the Fermi sea may undergo a deformation even in the spin-saturated system due to the difference of the Fermi surface between neutrons and protons; the momentum distributions of neutrons and protons may deform respectively to enlarge the overlapped region in the phase space, which effectively contributes to the np- pairing. They have shown the possibility of the deformation in a variational way; the Fermi sea of the majority of nucleons deforms in a prolate shape, while the minority in an oblate shape. Thus the deformation property of the Fermi seas looks very similar to our case. Nevertheless, note that our deformation is produced by the relativistic effect. Anyway it would be interesting to look further into the common feature.

It is to be noted that if the effective coupling constant is strong enough to lower the critical quark mass, spin polarization (magnetization) has potential to appear at rather moderate densities such as in the core of neutron stars, even though CSC weakly works against it.

From the above observations it is suggested that spin polarization does not compete with CSC but can coexist with it, unlike in ordinary superconductors of the electron system with the s-wave and spin-singlet pairing. This reflects the fact that internal degrees of freedom of the quark field, e.g., the color, flavor and Dirac indices, have rich structures to satisfy the antisymmetric constraint on the quark-pair field.

The possibility of the coexistent phase might also give a clue as for the origin of the superstrong magnetic field observed in magnetars. We roughly estimate the expected magnetic field when magnetars are assumed to be quark stars. The maximum dipole magnetic field at the star surface reads

$$B_{\max}=\frac{8\pi}{3}\mu_q n_q(\langle M_z\rangle/N_q), \tag{64}$$

with μ_q and n_q being the quark magnetic moment and the quark number density, respectively; e.g., for $\langle M_z\rangle/N_q \sim(10^{-3})$ and $n_q\sim O(1\ \mathrm{fm}^{-3})$, we find $B_{\max}\sim O(10^{15}\ \mathrm{G})$, which is comparable to that observed in magnetars [8,9].

In the present paper we have not taken into account chiral symmetry, which is one of the basic concepts in QCD. If chiral symmetry is restored at finite baryon number density, the quark mass becomes drastically smaller as density increases. In order to simulate it we have examined the quark mass dependence on spin polarization. In the future work we would like to consider an effect of the dynamical mass on the axial-vector self-energy.

ACKNOWLEDGMENTS

The present research of T.T. and T.M. is partially supported by the REIMEI Research Resources of Japan Atomic Energy Research Institute, and by the Japanese Grant-in-Aid for Scientific Research Fund of the Ministry of Education, Culture, Sports, Science and Technology (11640272, 13640282).

APPENDIX A: STRUCTURE OF SPINOR UNDER THE AXIAL-VECTOR MEAN-FIELD U_A

In this appendix we rewrite the spinor (23) in terms of the free quark one and the remainder characterized by U_A. We employ the free spinor $u_s(\boldsymbol{p})$ in which the two-component Pauli spinors are given as eigenvectors of the spin matrix σ_z,

$$u_\pm(\boldsymbol{p})=\begin{pmatrix}\sqrt{\epsilon_0+m}\,\xi_\pm\\ \dfrac{\sqrt{\epsilon_0-m}}{|p|}\boldsymbol{p}\cdot\boldsymbol{\sigma}\xi_\pm\end{pmatrix}\quad\text{with}\quad \xi_+=\begin{pmatrix}1\\0\end{pmatrix}\quad\text{and}\quad \xi_-=\begin{pmatrix}0\\1\end{pmatrix}, \tag{A1}$$

where $\epsilon_0=\sqrt{\boldsymbol{p}^2+m^2}$ and $\{\boldsymbol{\sigma}\}$ are the Pauli spin matrices.

The spinor $\phi_+(\boldsymbol{p})\equiv\phi_2(\boldsymbol{p})$ for the ''spin''-up state is decomposed as follows:

$$\frac{\beta_p(\Delta\,\epsilon-2U_A)+m(\delta\epsilon+2\beta_p)}{p_t^2p_z\mathcal{N}_+}\phi_+(\boldsymbol{p})=2\beta_p\sqrt{\epsilon_0+m}\left(\frac{\epsilon_+-\beta_p-U_A}{p_x+ip_y}u_+(\boldsymbol{p})-\frac{\beta_p+m}{p_z}u_-(\boldsymbol{p})\right)+\frac{\mathrm{Rem}_1(U_A)}{p_z(p_x+ip_y)}, \tag{A2}$$

where $\delta\epsilon \equiv \epsilon_- - \epsilon_+$, $\Delta\epsilon \equiv \epsilon_- + \epsilon_+$, and

$$\mathrm{Rem}_1(U_A) = \begin{pmatrix} p_z(\epsilon_+ - \beta_p - U_A)[\beta_p(\Delta\epsilon - 2U_A - 2\epsilon_0) + m\delta\epsilon] \\ -(p_x + ip_y)(\beta_p + m)[\beta_p(\Delta\epsilon - 2U_A - 2\epsilon_0) + m\delta\epsilon] \\ \delta\epsilon[(\epsilon_+ - \beta_p - U_A)p_z^2 + 2\beta_p^2(\beta_p + m)] - 2\beta_p(\beta_p + m)[(\epsilon_- - U_A)(\epsilon_+ - U_A) - \epsilon_0^2] \\ p_z(p_x + ip_y)(\beta_p + m)\delta\epsilon \end{pmatrix}. \tag{A3}$$

Note that the term $\mathrm{Rem}_1(U_A)$ vanishes in the limit, $U_A \to 0$. Thus one can find that $\phi_+(\boldsymbol{p})$ is a mixture of the free spinors even when $U_A = 0$.

A decomposition of the spinor $\phi_-(\boldsymbol{p}) \equiv \phi_1(\boldsymbol{p})$ for the "spin"-down state can also be done in a similar way,

$$\frac{\beta_p(\Delta\epsilon - 2U_A) + m(\delta\epsilon + 2\beta_p)}{p_t^2 p_z \mathcal{N}_-}\phi_-(\boldsymbol{p}) = 2\beta_p\sqrt{\epsilon_0 + m}\left(\frac{\epsilon_- + \beta_p - U_A}{p_x + ip_y}u_+(\boldsymbol{p}) + \frac{\beta_p - m}{p_z}u_-(\boldsymbol{p})\right) + \frac{\mathrm{Rem}_2(U_A)}{p_z(p_x + ip_y)}, \tag{A4}$$

where

$$\mathrm{Rem}_2(U_A) = \begin{pmatrix} p_z(\epsilon_- + \beta_p - U_A)[\beta_p(\Delta\epsilon - 2U_A - 2\epsilon_0) + m\delta\epsilon] \\ (p_x + ip_y)(\beta_p - m)[\beta_p(\Delta\epsilon - 2U_A - 2\epsilon_0) + m\delta\epsilon] \\ \delta\epsilon[(\epsilon_- + \beta_p - U_A)p_z^2 - 2\beta_p^2(\beta_p - m)] + 2\beta_p(\beta_p - m)[(\epsilon_- - U_A)(\epsilon_+ - U_A) - \epsilon_0^2] \\ -p_z(p_x + ip_y)(\beta_p - m)\delta\epsilon \end{pmatrix}. \tag{A5}$$

APPENDIX B: DECOMPOSITION OF $B_n(\mathbf{p})$ IN TERMS OF THE DIRAC GAMMA MATRICES

The operator $B_n(\boldsymbol{p})$ in Eq. (27) consists of some gamma matrices; it is a linear combination of $\boldsymbol{1}$, $\boldsymbol{\gamma}$, $\gamma_5\boldsymbol{\gamma}$, σ_{01}, and σ_{02} in the diquark field $\overline{\psi_c}B_n\psi = \psi^T C B_n \psi$. The last two matrices give the tensor diquark fields, while these terms have no influence on the gap equation (38) due to axial symmetry of the Fermi seas around the p_z axis: the integration of $B_n(\boldsymbol{p})$ with respect to the azimuthal angle ϕ_p in Eq. (38) gives

$$\begin{aligned}\tilde{B}_n(\boldsymbol{p}) &\equiv \int_0^{2\pi}\frac{\mathrm{d}\phi_p}{2\pi}B_n(\boldsymbol{p}) \\ &= \frac{p_t}{4|\epsilon_n(\boldsymbol{p})|\beta_p}[(-1)^n p_z\gamma_3 + (-1)^n m\boldsymbol{1} + \beta_p\gamma_5\gamma_3].\end{aligned} \tag{B1}$$

Thus tensor terms disappear because they are proportional to $\exp(i\phi_p)$ in $B_n(\boldsymbol{p})$.

The first term on the right-hand side also has no contribution after symmetric integration with respect to p_z. The remainders $\{\mathbf{1}, \gamma_5\gamma_3\}$ imply the pseudoscalar ($J^P = 0^-$) and vector ($J^P = 1^-$) diquark pairings in terms of the notation in Ref. [2]. Please note that the CSC gap (B1) results in a linear combination of different angular momentum pairs 0^- and 1^- because of the lack of rotation symmetry.

Since the diquark fields $\psi^T C(\mathbf{1}, \gamma_5\gamma_3)\psi$ contain the off-diagonal matrices which connect the lower component with the upper one of the Dirac spinors, these pairings vanish in the nonrelativistic limit or in the limit $m \to \infty$. Hence $B_n(\mathbf{p})$ resembles P-wave pairing as is seen in Eq. (50), although it has no correspondence in the nonrelativistic limit: the gap function for Eq. (B1) has the nodes (vanishing at $\theta = 0, \pi$) due to the factor p_t, which is similar to ^3P pairing in the liquid ^{3}He-A phase, but these nodes are entirely attributed to the genuine relativistic effect. This property survives even in the limit $U_A \to 0$.

From Eq. (B1) we can also obtain the relation appearing in Eq. (40),

$$\gamma_\mu\gamma_0\tilde{B}_n(\boldsymbol{p})\gamma_0\gamma^\mu = 2\tilde{B}_n(\boldsymbol{p}) + 2m\{m + (-1)^n\beta_p\}. \tag{B2}$$

APPENDIX C: PARAMETRIZATION OF THE GAP FUNCTION

In this appendix we derive the parametrization (47). The gap equation (41) is expanded as

$$\begin{aligned}\Delta_\pm(k) = \frac{2}{3}\tilde{g}^2\int\frac{\mathrm{d}^3p}{(2\pi)^3}\frac{k_t}{2\epsilon_\pm(k)}\Bigg[\frac{p_t}{\epsilon_+(p)}\left(\pm\frac{2m^2}{\beta_k\beta_p} + 1\right) \\ \times\frac{\Delta_+(p)}{2E_+(p)} + \frac{p_t}{\epsilon_-(p)}\left(\mp\frac{2m^2}{\beta_k\beta_p} + 1\right)\frac{\Delta_-(p)}{2E_-(p)}\Bigg].\end{aligned} \tag{C1}$$

Introducing $\hat{\Delta}_\pm(k)$ through the equation

$$\Delta_\pm(k) = \frac{k_t}{\epsilon_\pm(k)}\hat{\Delta}_\pm(k), \tag{C2}$$

we obtain the "gap" equation for $\hat{\Delta}_\pm(k)$,

$$\hat{\Delta}_{\pm}(k)=\frac{2}{3}\tilde{g}^2\int\frac{d^3p}{(2\pi)^3}\frac{p_t^2}{4}\times\left[\mp\frac{2m^2}{\beta_k\beta_p}\left(\frac{\hat{\Delta}_-(p)}{\epsilon_-(p)^2E_-(p)}-\frac{\hat{\Delta}_+(p)}{\epsilon_+(p)^2E_+(p)}\right)+\frac{\hat{\Delta}_-(p)}{\epsilon_-(p)^2E_-(p)}+\frac{\hat{\Delta}_+(p)}{\epsilon_+(p)^2E_+(p)}\right]. \tag{C3}$$

Then we find the following properties:

$$\hat{\Delta}_-(k)+\hat{\Delta}_+(k)=2F \quad \text{and} \quad \hat{\Delta}_-(k)-\hat{\Delta}_+(k)=2R\times\frac{m}{\beta_k}, \tag{C4}$$

where F (R) is a constant which characterizes the symmetric (asymmetric) combinations of the gap functions $\hat{\Delta}_{\pm}$. Thus we can further parametrize $\hat{\Delta}_s(k)$ as

$$\hat{\Delta}_{\pm}(k)=\mp\frac{m}{\beta_k}R+F. \tag{C5}$$

Substituting the above formula into Eq. (C3), one can obtain the coupled equations for F and R, Eqs. (48) and (49).

APPENDIX D: FIERZ TRANSFORMATION

We present the Fock exchange energy term by the OGE interaction by the use of the Fierz transformation. The Green function with vertices on the right-hand side of Eq. (14) can be expanded as

$$\sum_a[\Gamma_a iG_{11}(p)\Gamma_a]_{ij}=\sum_a(\Gamma_a)_{ii'}\langle\psi(p)_{i'}\bar{\psi}(p)_{j'}\rangle(\Gamma_a)_{j'j}=\sum_{ab}C_{ab}(\Gamma_b)_{ij}\mathrm{Tr}(G_{11}\Gamma_b) \tag{D1}$$

with

$$\Gamma_a\equiv\gamma_\mu\otimes\mathbf{1}_{flavor}\otimes\lambda_{color}$$

and

$$(\Gamma_a)_{ii'}(\Gamma_a)_{j'j}=\sum_b C_{ab}(\Gamma_b)_{ij}(\Gamma_b)_{j'i'}, \tag{D2}$$

where $\{C_{ab}\}$ are coefficients of a Fierz transformation (D2) for the Dirac matrices, the identity matrix in the flavor space, and the Gell-Mann matrices in the color space,

$$(\gamma_\mu)_{ii'}(\gamma^\mu)_{j'j}=\delta_{ij}\delta_{j'i'}-\frac{1}{2}(\gamma_\mu)_{ij}(\gamma^\mu)_{j'i'}-\frac{1}{2}(\gamma_5\gamma_\mu)_{ij}(\gamma_5\gamma^\mu)_{j'i'}+(i\gamma_5)_{ij}(i\gamma_5)_{j'i'}, \tag{D3}$$

$$\delta_{ii'}\delta_{j'j}=\frac{1}{2}\left[\frac{2}{N_f}\delta_{ij}\delta_{j'i'}+(\tau_a)_{ij}(\tau_a)_{j'i'}\right], \tag{D4}$$

$$(\lambda_c)_{ii'}(\lambda_c)_{j'j}=\frac{2}{N_c^2}(N_c^2-1)\delta_{ij}\delta_{j'i'}-\frac{1}{N_c}(\lambda_c)_{ij}(\lambda_c)_{j'i'}. \tag{D5}$$

It should be noted that there appears no tensor term in Eq. (D3) due to chiral symmetry in QCD. Thus, e.g., the coefficient for the color-singlet axial-vector self-energy reads $-4/9$ for $N_f=2$ and $N_c=3$.

We also present a Fierz transformation for diquark fields. The right-hand side of Eq. (15) can be expanded in a similar way for G_{11},

$$\sum_a[\bar{\Gamma}_aG_{21}(p)\Gamma_a]_{ij}=\sum_a(C\Gamma_a^TC^{-1})_{ii'}\langle\psi_c(p)_{i'}\bar{\psi}(p)_{j'}\rangle(\Gamma_a)_{j'j}=\sum_a(C)_{ik}(\Gamma_a)_{i'k}\langle\bar{\psi}(-p)_{i'}\bar{\psi}(p)_{j'}\rangle(\Gamma_a)_{j'j}=\sum_{ab}f_{ab}\mathrm{Tr}[G_{21}(p)C^{-1}\Gamma_b^TC^{-1}](C\Gamma_b^TC^T)_{ij} \tag{D6}$$

with

$$(\Gamma_a)_{i'k}(\Gamma_a)_{j'j}=\sum_b f_{ab}(\Gamma_bC^*)_{i'j'}(C\Gamma_b)_{jk}, \tag{D7}$$

where $\{f_{ab}\}$ are coefficients of a Fierz transformation (D7) and are explicitly given as

$$(\gamma_\mu)_{i'k}(\gamma^\mu)_{j'j}=(C^*)_{i'j'}(C)_{jk}-\frac{1}{2}(\gamma_\mu C^*)_{i'j'}(C\gamma^\mu)_{jk}-\frac{1}{2}(\gamma_\mu\gamma_5C^*)_{i'j'}(C\gamma^\mu\gamma_5)_{jk}+(iC^*\gamma_5)_{i'j'}(iC\gamma_5)_{jk}, \tag{D8}$$

$$\delta_{i'k}\delta_{j'j}=\frac{1}{2}\left[\frac{2}{N_f}\delta_{i'j'}\delta_{jk}+(\tau_a)_{i'j'}(\tau_a)_{jk}\right], \tag{D9}$$

$$(\lambda_c)_{i'k}(\lambda_c)_{j'j}=\left(1-\frac{1}{N_c}\right)\left[\frac{2}{N_c}(\delta)_{i'j'}(\delta)_{jk}+(\lambda_c^S)_{i'j'}(\lambda_c^S)_{jk}\right]-\left(1+\frac{1}{N_c}\right)(\lambda_c^A)_{i'j'}(\lambda_c^A)_{jk}, \tag{D10}$$

where $\{\lambda_c^{S(A)}\}$ are symmetric (antisymmetric) matrices of $\{\lambda_c\}$. The present gap function, $\Delta(\mathbf{p})=\Sigma_nB_n(\mathbf{p})\Delta_n(\mathbf{p})$, which is a linear combination of the gamma matrices, can be obtained by taking projection on $B_n(\mathbf{p})$.

[1] B.C. Barrois, Nucl. Phys. **B129**, 390 (1977).
[2] D. Bailin and A. Love, Phys. Rep. **107**, 325 (1984).
[3] M. Iwasaki and T. Iwado, Phys. Lett. B **350**, 163 (1995); R. Rapp, T. Schäfer, E. Shuryak, and M. Velkovsky, Phys. Rev. Lett. **81**, 53 (1998); M. Alford, K. Rajagopal, and F. Wilczek, Phys. Lett. B **422**, 247 (1998); D.T. Son, Phys. Rev. D **59**, 094019 (1999); N. Evans, S. Hsu, and M. Schwetz, Phys. Lett. B **449**, 281 (1999); R.D. Pisarski and D.H. Rischke, Phys. Rev. D **61**, 074017 (2000); W.E. Brown, J.T. Liu, and H. Ren, *ibid.* **61**, 114012 (2000); V.A. Miransky, I.A. Shovkovy, and L.C.R. Wijewardhana, *ibid.* **62**, 085025 (2000); for a recent review of color superconductivity, see M. Alford, Annu. Rev. Nucl. Part. Sci. **51**, 131 (2001), and references therein.
[4] J. R. Schrieffer, *Theory of Superconductivity* (Benjamin, New York, 1964).
[5] M. Alford, K. Rajagopal, and F. Wilczek, Nucl. Phys. **B537**, 443 (1999); J. Berges and K. Rajagopal, *ibid.* **B538**, 215 (1999); T.M. Schwarz, S.P. Klevansky, and G. Papp, Phys. Rev. C **60**, 055205 (1999); D. Ebert, V.V. Khudyakov, V.Ch. Zhukovsky, and K.G. Klimenko, Phys. Rev. D **65**, 054024 (2002).
[6] L.N. Buaevskii *et al.*, Adv. Phys. **34**, 175 (1985).
[7] S.S. Sexena *et al.*, Nature (London) **406**, 587 (2000); C. Pfleiderer *et al.*, *ibid.* **412**, 58 (2001); N.I. Karchev *et al.*, Phys. Rev. Lett. **86**, 846 (2001); K. Machida and T. Ohmi, *ibid.* **86**, 850 (2001).
[8] B. Paczyński, Acta Astron. **41**, 145 (1992); R.C. Duncan and C. Thompson, Astrophys. J. Lett. **392**, L19 (1992); C. Thompson and R.C. Duncan, Mon. Not. R. Astron. Soc. **275**, 255 (1995).
[9] C. Kouveliotou *et al.*, Nature (London) **393**, 235 (1998); K. Hurley *et al.*, Astrophys. J. Lett. **510**, L111 (1999).
[10] For a review, see G. Chanmugam, Annu. Rev. Astron. Astrophys. **30**, 143 (1992).
[11] T. Tatsumi, Phys. Lett. B **489**, 280 (2000).
[12] J.C. Collins and M.J. Perry, Phys. Rev. Lett. **34**, 1353 (1975).
[13] T. Maruyama and T. Tatsumi, Nucl. Phys. **A693**, 710 (2001).
[14] Y. Nambu, Phys. Rev. **117**, 648 (1960).
[15] J.I. Kapusta, *Finite-Temperature Field Theory* (Cambridge University Press, Cambridge, England, 1989); M. LeBellac, *Thermal Field Theory* (Cambridge University Press, Cambridge, England, 1996).
[16] G. Ripka, *Quarks Bound by Chiral Fields* (Oxford University Press, Oxford, 1997).
[17] For example, see K. Yoshida, *Theory of Magnetism* (Springer-Verlag, Berlin, 1996).
[18] Y. Nambu and G. Jona-Lasinio, Phys. Rev. **122**, 345 (1961); **124**, 246 (1961).
[19] M. Buballa, J. Hošek, and M. Oertel, Phys. Rev. D **65**, 014018 (2002); T. Fugleberg, *ibid.* **67**, 034013 (2003).
[20] M. Alford, J. Berges, and K. Rajagopal, Nucl. Phys. **B558**, 219 (1999).
[21] R.D. Pisarski and D.H. Rischke, Phys. Rev. D **60**, 094013 (1999).
[22] For example, see D. Vollhardt and P. Wölfle, *The Superfluid Phases of Helium 3* (Taylor and Francis, London, 1990).
[23] R. Tamagaki, Prog. Theor. Phys. **44**, 905 (1970); M. Hoffberg, A.E. Glassgold, R.W. Richardson, and M. Ruderman, Phys. Rev. Lett. **24**, 775 (1970).
[24] T. Hatsuda and T. Kunihiro, Phys. Rep. **247**, 221 (1994).
[25] A.A. Abrikosov, *Fundamentals of the Theory of Metals* (North Holland, Amsterdam, 1988).
[26] H. Müther and A. Sedrakian, Phys. Rev. Lett. **88**, 252503 (2002).